Weld World (2016) 60:623–638
DOI 10.1007/s40194-016-0325-9

RESEARCH PAPER

Effect of hydrogen on mechanical properties of heat affected zone of a reactor pressure vessel steel grade

Michael Rhode[1] · **Joerg Steger**[1] · **Enrico Steppan**[1] · **Thomas Kannengiesser**[1]

Received: 6 October 2015 / Accepted: 1 March 2016 / Published online: 18 March 2016

Abstract The steel grade 20MnMoNi5-5 (according to German DIN standard or 16MND5 according to French AFNOR standard) is widely applied in (weld) fabrication of reactor pressure vessel components. Thus, a wide range of welding technologies (like submerged arc welding (SAW) or tungsten inert gas (TIG)) is used resulting in different heat affected zone (HAZ) microstructures. During weld fabrication, the weld joints may take up hydrogen. Especially, the HAZ shows an increased susceptibility for a degradation of the mechanical properties in presence of hydrogen. In addition, the hydrogen-assisted degradation of mechanical properties is influenced by three main local factors: hydrogen concentration, microstructure, and load condition. Hence, the base material (BM) and two different simulated non-tempered as-quenched HAZ microstructures were examined using hydrogen-free and hydrogen-charged tensile specimens. The results indicate that the effect of hydrogen on the degradation is significantly increased in case of the HAZ compared to the BM. In addition, hydrogen has remarkable effect in terms of reduction of ductility. It was ascertained that the degradation of the mechanical properties increases in the order of BM, bainitic HAZ, and the martensitic HAZ. Scanning electron microscope (SEM) investigation showed a distinct change of the fracture topography depended on the microstructure with increasing hydrogen concentration in case of the as-quenched HAZ microstructures.

Keywords (IIW Thesaurus) Pressure vessel steels · Heat affected zone · Hydrogen · Hydrogen embrittlement · Low alloy steels · Mechanical properties

Recommended for publication by Commission C-II Arc welding and Filler Metals

✉ Michael Rhode
michael.rhode@bam.de

[1] BAM Federal Institute for Materials Research and Testing, Berlin, Germany

1 Introduction

The low alloyed bainitic 20MnMoNi5-5 steel grade is one of the most important steel grades for welding fabrication of heavy components in nuclear industry [1–3]. Common welding techniques like tungsten inert gas (TIG) or submerged arc welding (SAW) are applied in weld fabrication of the nuclear island components like the reactor pressure vessel (RPV) in pressurized water reactors [4, 5]. In addition, different microstructures occur in the heat affected zone (HAZ) (for example bainite or martensite) which are dependent on the chemical composition, peak temperature, and subsequent cooling condition (and tempering/annealing effects). For example, Kuo et al. [6] reported for A533B steel for cooling time from 800 to 500 °C ($t_{8/5}$) of 10 s a mixture of bainite and martensite. In case of $t_{8/5}$ time of 20 s, a mostly bainitic microstructure occurs. Hence, dependent on the mentioned thermal cycle parameters, more or less refined or coarse grains with bainite, martensite, or mixture microstructure appear in the HAZ of welded joints of bainitic RPV steels [7]. However, in general, weld joints of steels can show hydrogen uptake during welding fabrication from numerous sources [8, 9]. For example, in case of submerged arc welding (SAW), hydrogen can be picked-up in the weld pool by moisture of the flux [9] or in general from hydrogen-containing compounds of surface

contaminants (oil, grease, etchants, etc.) on the steel surface [10]. In fact, hydrogen causes a degradation of the mechanical properties. This degradation mostly appears in terms of reduced ductility (elongation, reduction in area, toughness) [11]. However, this degradation effect in presence of hydrogen increases with increasing tensile strength of the steels [12, 13]. This becomes essential for the HAZ due to the microstructure change if martensite is formed as result of the thermal cycle [6, 14]. In general, the HAZ of Mn-Mo-Ni steel shows increased tensile strength. Hence, the knowledge of a certain degradation behavior in presence of hydrogen is extremely important for evaluation of possible susceptibility of the different microstructures.

Especially, in case of RPV steels, hydrogen concentrations of 2.5 to 4.0 ppm are sufficient for a remarkable degradation of the mechanical properties in terms of ductility [15, 16]. Several studies on hydrogen degradation of mechanical properties were carried out for base material (BM) grades without detailed consideration of microstructure features in the heat affected zone (HAZ) [11, 15–18]. Even in hydrogen-free condition, the coarse-grain HAZ is regarded as the most sensitive microstructure of RPV steels in terms of degradation of mechanical properties (toughness) [14, 19]. Under consideration of the detrimental influence of hydrogen on degradation of mechanical properties, the HAZ needs special focus which was investigated for the HAZ of Cr-Mo-V low alloyed pressure vessel steels [20]. Nevertheless, a quantitative assessment in terms of hydrogen concentration (related to a certain degradation level) is less available for HAZ microstructures of RPV steels. In addition, certain susceptibility for hydrogen-assisted degradation is influenced by the local hydrogen concentration and load condition.

Thus, it is necessary to separate the mentioned effects for each microstructure (BM vs. HAZ). Thus, two different HAZ microstructures were thermally simulated by defined time-temperature cycle from bainitic low alloyed Mn-Mo-Ni steel with two different cooling conditions: a non-tempered bainitic microstructure representing achieved by long cooling time and an as-quenched martensitic microstructure representing a fast cooling time. Subsequently, tensile specimens were machined from the simulated specimens and electrochemically hydrogen-charged to examine the degradation effect on a certain hydrogen concentration determined with carrier gas hot extraction (CGHE). Nevertheless, hydrogen trapping (i.e., local hydrogen concentration) vs. grain size (in case of thermal cycling) is a very complex phenomenon [21, 22] which can be also related to a certain tempering temperature [23]. In scope of the mechanical properties, the peak temperature for simulation of the HAZ microstructures was kept constant. Hence, a possible grain size effect (for example pinning effect of stable precipitates on austenite grain growth like shown in [24]) on the degradation is not examined in particular.

Table 1 Chemical composition of BM

C	Mn	Mo	Ni	Al	Si	Cr	Cu	V	P + S	Fe
0.22	1.49	0.50	0.64	0.02	0.24	0.18	0.05	0.002	0.004	Balance

2 Materials and methods

2.1 Material

The 20MnMoNi5-5 (according to German standard and 16MND5 in French standard) is widely applied in nuclear components fabrication subjected to welding [1–3]. The BM grade was in the quenched and tempered (Q + T) condition with an average hardness of 210 HV5. Thus, the BM is austenitized at 900 °C followed by water-quenching and tempering at 640 °C with final air-cooling to ambient temperature. Table 1 shows the chemical composition of the as-received condition of the steel grade. Table 2 shows the corresponding mechanical properties at room temperature.

2.2 Thermal cycle for simulated HAZ microstructure

To obtain homogenous microstructure for HAZ specimens, the BM grade was subjected to specified heat treatment cycles corresponding to different welding processes. For the evaluation of the hydrogen effects on the mechanical properties, two different heat-affected microstructures were simulated with different cooling conditions: increased cooling rate for the as-quenched martensitic condition and a low cooling rate for a mostly bainitic (non-tempered) microstructure. Both microstructures were examined in the as-quenched condition. Thus, the specimens were heated to the peak temperature using inductive heating device and subsequent gas-quenching in inert gas flow. The inductive heating device uses an alternating high-frequency (HF) 250-kHz electromagnetic field with an applied maximum power of 3 kW (HF-output). The applied heat treatment parameters are illustrated in

Table 2 Mechanical properties of BM

$R_{p0,2}$ in MPa	R_m in MPa	A in %
590	673	22

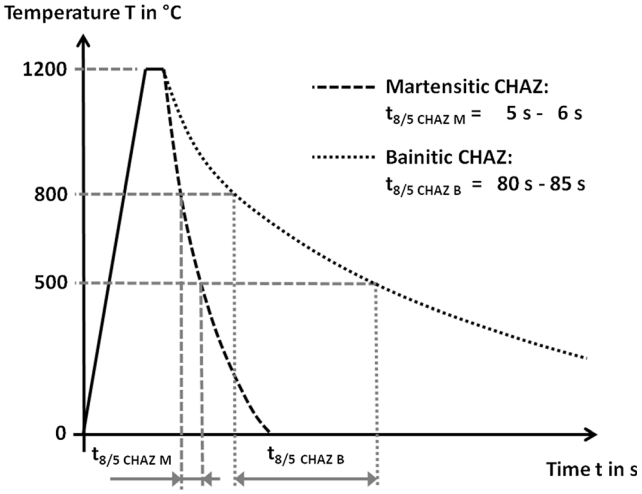

Fig. 1 Conducted heat treatment conditions

Fig. 1. The specimens for simulation of the time-temperature cycle had a length of 80 mm and a diameter of 6 mm (martensitic HAZ) and 8 mm (bainitic HAZ).

The BM was heated within 20 s to a peak temperature of 1200 °C. This temperature was hold for approximately 5–6 s. Due to the chosen peak temperature, this range represents a typical (coarse-grained) heat affected zone (CGHAZ) microstructure in RPV steels [6, 14, 25]. For temperature measurement, high-temperature thermocouple (type K) was applied in the center region of the specimen perpendicular to the inductor coil. In addition, a color pyrometer was applied for reference measurement. Previous measurements with additional thermocouples distributed in longitudinal specimen axis ensured a nearly homogenous temperature distribution in the entire heat-treated specimen volume. In the following, the two thermally simulated microstructures are indicated with "M HAZ" representing the as-quenched martensitic microstructure and "B HAZ" representing the non-tempered bainitic HAZ. The hardness of the martensitic HAZ is approximately 448 and 276 HV5 for the bainitic HAZ, respectively. The corresponding fine-grained heat-affected microstructures will be reported in an additional paper. The microstructure of the BM is shown in Fig. 2a. Due to thermal cycling, the subsequent fast cooling with a corresponding cooling time $t_{8/5}$ of 5 to 6 s leads to a mostly as-quenched martensitic microstructure (Fig. 2b) with

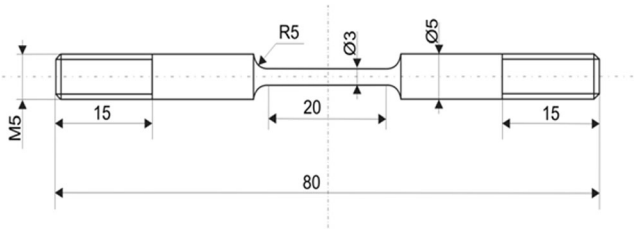

Fig. 3 Tensile specimen geometry

increased hardness. This high cooling time was chosen to simulate a mostly martensitic microstructure as the worst case scenario in terms of hydrogen-affected degradation of hardened HAZ microstructure. For example, comparable cooling times were investigated by Kuo et al. [6] (approx. 5 s). In contrast, a slow cooling condition with a respective $t_{8/5}$ cooling time of 80 to 85 s leads to mostly bainitic microstructure (Fig. 2c). This extended cooling time was chosen for the evaluation of the microstructure influence on the hydrogen-affected degradation considering a non-tempered as-welded bainitic HAZ microstructure. In addition, the occurring microstructures for such high cooling times were investigated by Yang and Liou [25]. Nevertheless, the effect of hydrogen on such microstructures is missing, and that is the scope of the present study.

2.3 Tensile testing

The tensile tests were performed to determine the hydrogen degradation effects on mechanical properties of the mentioned microstructures. An Instron 8520 test facility was used with a constant load velocity of 1 mm/min. The yield strength (YS) and the ultimate tensile strength (UTS) were calculated from the recorded tensile force. The elongation was measured with a clip gauge during testing. All data were captured and stored with a triggered data logging system. After the tensile test, the reduction in area was determined using optical microscopy with five-time magnification and a digital image capture system. After charging, the specimens were stored immediately in liquid nitrogen at −196 °C in order to prevent hydrogen effusion until the tensile test starts. Before testing, each specimen was defrosted in acetone for ca. 60 s to achieve ambient temperature. Figure 3 shows the used round tensile specimen geometry.

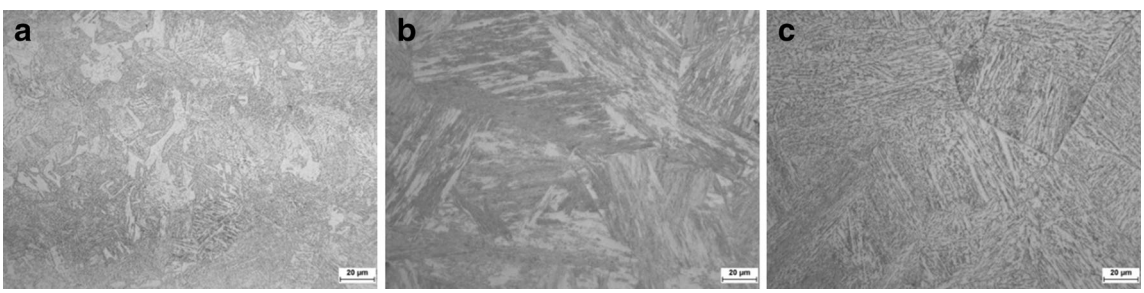

Fig. 2 **a** BM, (**b**) M HAZ, and (**c**) B HAZ

After the tensile test, one half of the fractured specimen was stored in liquid nitrogen again for the later analysis of the corresponding hydrogen concentration in the specimen. The other half of the specimen was used for fractography analysis by scanning electron microscope (SEM).

2.4 Hydrogen charging

The hydrogen charging was performed with cathodic charging procedure using 0.1 M H_2SO_4 acid solution with addition of 12 mg/l $NaAsO_2$ as recombination poison preventing the hydrogen from recombination to molecular form. The galvanostatic charging (constant current density during charging) was used to obtain different hydrogen concentrations by varying the charging current density. Platinum electrode (Pt 1800 SI Analytics) was anode, and the specimen was cathode. This procedure was already presented in [26]. Before charging, each specimen was cleaned in acetone using an ultrasonic bath and rinsed in inert nitrogen gas flow. Previous hydrogen-charging tests were conducted with cylindrical BM and B and M HAZ calibration specimens (3 mm diameter, 20 mm length) to ensure full hydrogen saturation of the later tensile specimens. Thus, the specimens were charged at least for duration of minimum 24 h. Table 3 shows the used charging current densities for the hydrogen charging.

2.5 Hydrogen detection

The corresponding hydrogen concentration in the specimens was measured using a Bruker JUWE H-mat 221. This device uses the carrier gas hot extraction (CGHE) technique with thermal conductivity device (TCD) to determine the effusing hydrogen from the specimens. Thus, the specimen is heated up in a glass plunger in inert gas flow. The effusing hydrogen changes the thermal conductivity of the inert gas and is recorded with the TCD sensor. The ex-ante calibration with different defined amounts of hydrogen allows exact results. The CGHE principle and calibration was previously reported [27]. Previous tests with the calibration specimens of the hydrogen-charging tests were subjected to different testing temperatures. It was found that the hydrogen amount in the specimen was similar between a testing temperature of 100 and 800 °C. This means possible hydrogen-trapping effects in this temperature range can be neglected, and the used temperature for hydrogen collection was fixed at 800 °C.

Table 3 Charging current densities

Grade	Level I mA/cm^2	Level II mA/cm^2	Level III mA/cm^2
BM	0.6	10	20
M HAZ	0.6	1.5	10
B HAZ	0.6	1.5	10

For practical reasons, the hydrogen concentration data in this study is given in ml/100 g Fe. This unit describes the dissolute hydrogen amount in milliliter referred to 100 g specimen weight of the examined steel grade. This unit is the common value for describing hydrogen concentration in weld joints [28]. For comparison, 1 ml/100 g Fe corresponds to 0.91 or 1 ppm to 1.1 ml/100 g Fe. In average, the maximum time from transfer from liquid nitrogen, defrosting, mounting, and testing of the specimens was less than 4 min in hydrogen-charged condition. Hence, the determined hydrogen concentration represents the remaining hydrogen in the specimen after the tensile test. Accompanying tests with hydrogen-charged cylindrical specimens showed a maximum hydrogen loss of approximately 10 %. This was also shown in [26]. Thus, the remaining hydrogen is the specimen after tensile test is labeled “diffusible” in accordance to the ISO 3690 [28]. It has to be mentioned that this experimentally determined hydrogen concentration cannot be compared directly to measurements for weld metal described in the ISO standard. The reason is the different time between the storage in liquid nitrogen and hydrogen determination.

3 Results

3.1 Mechanical properties

3.1.1 Ultimate tensile strength and yield strength

Figure 4 shows the obtained data for the ultimate tensile strength R_m (UTS) and the yield strength $R_{p0,2}$ (YS) in MPa for the BM grade (Fig. 4a), the B HAZ (Fig. 4b), and the M HAZ (Fig. 4c). As shown in Fig. 4a, the BM showed no remarkable degradation of tensile properties up to a hydrogen concentration of 3 ml/100 g Fe. A similar behavior was determined for the B HAZ (Fig. 4b) but an increased YS and UTS in hydrogen-free condition. This is due to the higher hardness as consequence of the thermal cycle. In hydrogen-charged condition, no distinct degradation effect is observed. The non-tempered bainitic HAZ microstructure shows sufficient mechanical tensile properties to the maximum determined hydrogen concentration of 4 ml/100 g Fe. Compared to the BM (and the B HAZ), the as-quenched M HAZ microstructure (Fig. 4c) showed the highest YS and UTS in the hydrogen-free condition. This is due to the fast cooling condition leading to a martensitic microstructure accompanied by increased hardness of approx. 440 HV. In the hydrogen-charged condition, the M HAZ showed significant degradation of the material properties. For example, the as-quenched M HAZ showed a decrease of UTS from the initial 1300 MPa to the range of 600 to 800 MPa at 3 ml/100 g Fe. At this hydrogen

concentration, the, UTS has the same value like the YS. Hence, the ductility is nearly decreased to zero.

3.1.2 Ductility

Elongation to fracture In general, the ductility of the different microstructures show an increased degradation behavior compared to the UTS and YS. Figure 5 shows the determined data for the elongation to fracture of the BM (Fig. 5a), the non-tempered B HAZ (Fig. 5b), and the as-quenched M HAZ (Fig. 5c). As shown in Fig. 5a, the BM shows excellent

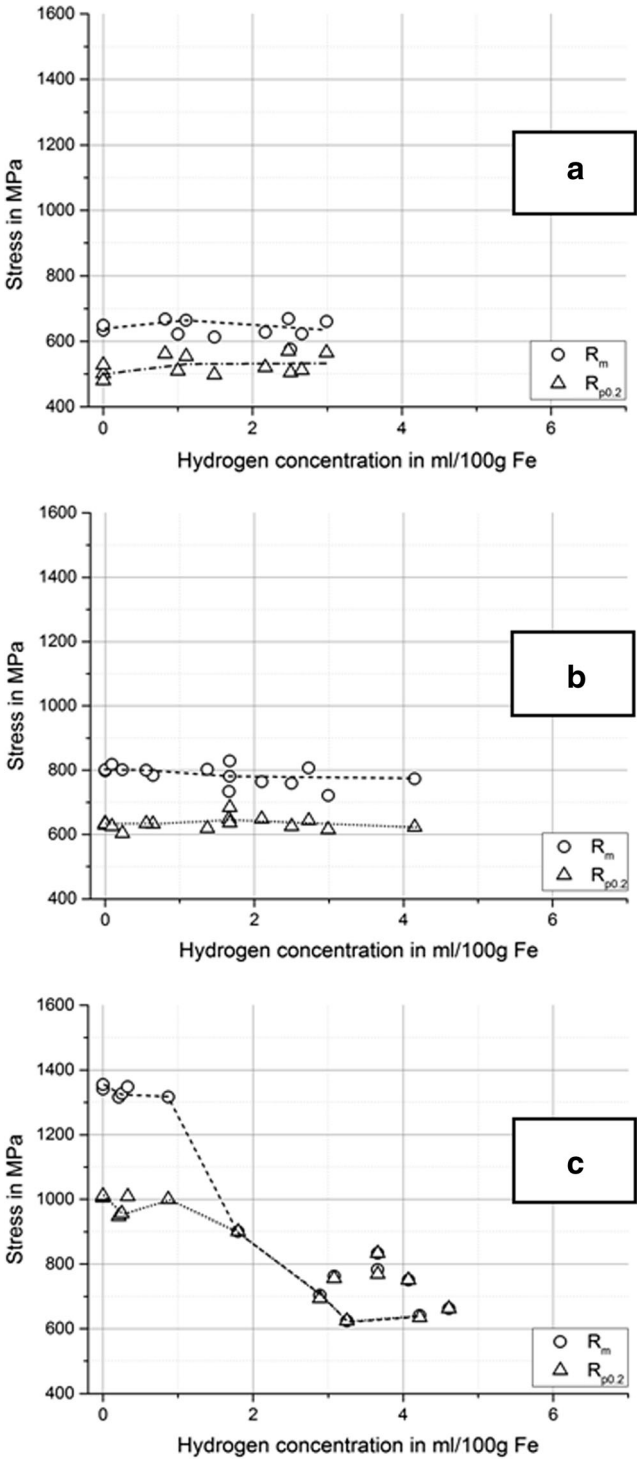

Fig. 4 R_m and $R_{p0,2}$ of BM (**a**), B HAZ (**b**), and M HAZ (**c**)

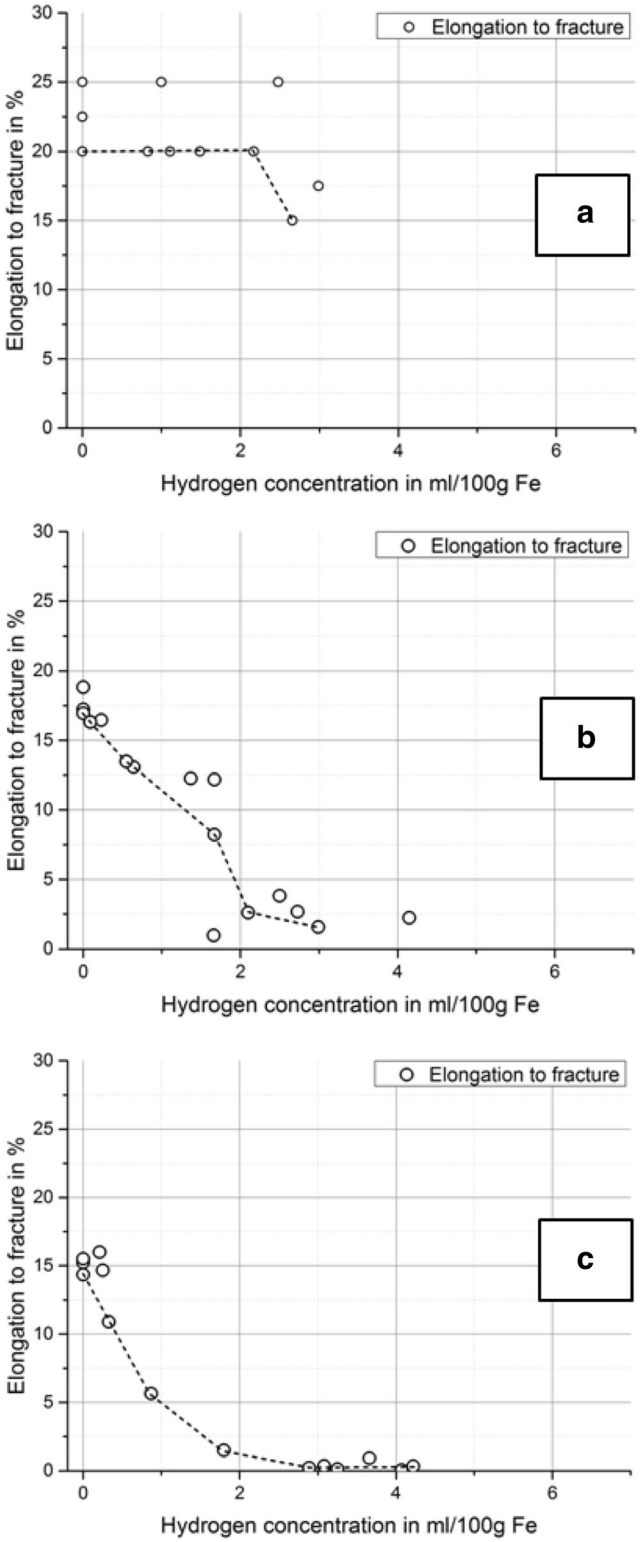

Fig. 5 Elongation to fracture of BM (**a**), B HAZ (**b**), and M HAZ (**c**)

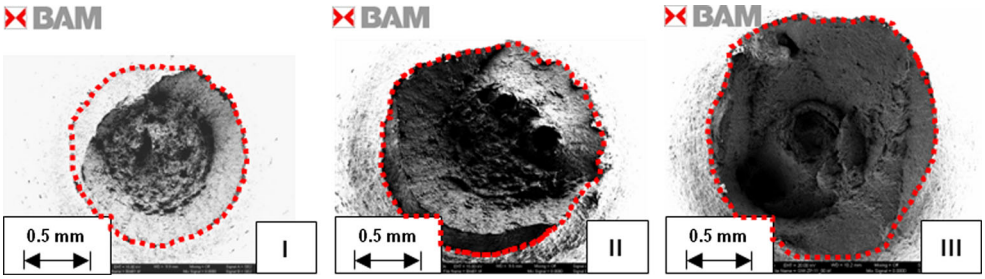

Fig. 6 BM: (*I*)—Uncharged, (*II*)—1.1 ml/100 g Fe, and (*III*)—3.0 ml/100 g Fe

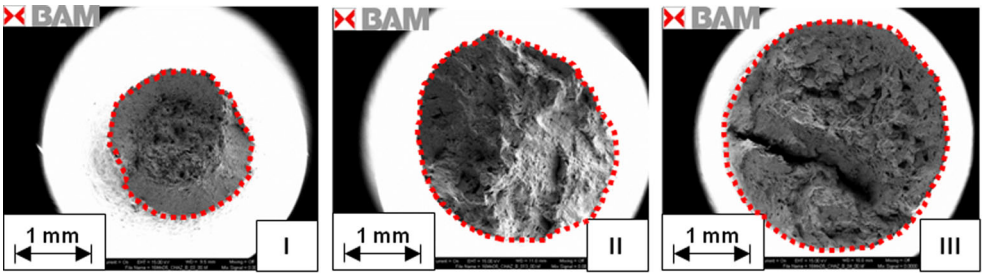

Fig. 7 B HAZ: (*I*)—Uncharged, (*II*)—1.6 ml/100 g Fe, and (*III*)—3.0 ml/100 g Fe

ductility. In hydrogen-charged condition, the elongation to fracture remains above 15 % at hydrogen concentration of 3 ml/100 g Fe compared to 20 % in uncharged condition.

In comparison to the (Q + T) BM, the non-tempered B HAZ (Fig. 5b) shows distinct change of the ductility at hydrogen concentration of approx. 2 ml/100 g Fe. In this case, the elongation to fracture decreases from 12 to below 4 %. Compared to the B HAZ, the as-quenched M HAZ (Fig. 5c) microstructure shows the strongest degradation in terms of decreased ductility in the hydrogen-charged condition. This expressed by a significant decrease of the elongation to fracture from 15 % in the uncharged condition to 5 % in the hydrogen-charged condition at of 1 ml/100 g Fe. At hydrogen concentration of 2 ml/100 g Fe, the elongation to fracture is nearly zero.

Reduction in area The reduction in area can be applied as evaluation parameter of the degradation effect in the hydrogen-charged condition. Figures 6, 7, and 8 show an overview of the fracture area of the BM (Fig. 6), the B HAZ (Fig. 7), and the M HAZ (Fig. 8). Different hydrogen concentrations are marked with I, II, and III corresponding to the charging conditions (I–III):

- Condition I—Uncharged,
- Condition II—Moderate hydrogen charging (0.9 to 1.6 ml/100 g Fe), and
- Condition III—High hydrogen charging (1.8 to 3.0 ml/100 g Fe).

From Figs. 6, 7, and 8, it is clearly seen that there is a general tendency for increasing degradation of the mechanical properties with increasing hydrogen concentration. All examined microstructures show an increasing diameter of the remaining fracture surface (corresponding to a decreased calculated reduction in area) in case of the hydrogen-free condition (I) compared to the hydrogen-charged conditions II and III. By taking into account the different scales of Fig. 6 (0.5 mm) and Fig. 7 and 8 (each corresponds to 1.0 mm), it is seen that the degradation effect is increased for the HAZ microstructures compared to the BM. In case of the M HAZ, a low hydrogen concentration of 0.9 ml/100 g Fe leads to an increase of the corresponding fracture surface diameter from 1.8 to nearly 3.0 mm.

Hence, hydrogen has a distinct effect on the ductility expressed by a decreased elongation to fracture and the reduction in area. The corresponding calculated values for the

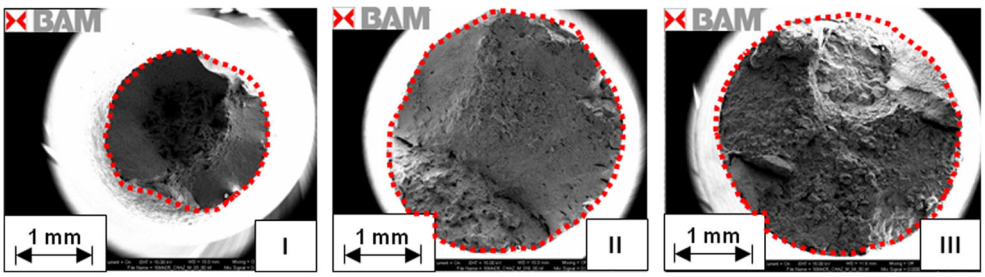

Fig. 8 M HAZ: (*I*)—Uncharged, (*II*)—0.9 ml/100 g Fe, and (*III*)—1.8 ml/100 g Fe

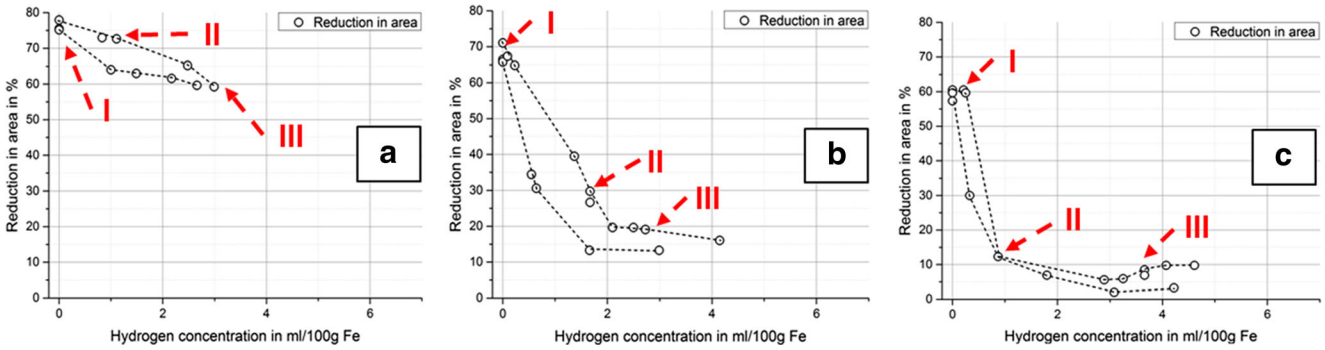

Fig. 9 Reduction in area of BM (**a**), B HAZ (**b**), and M HAZ (**c**)

reduction in area are shown in Fig. 9 for the BM in part (a), the B HAZ in part (b), and the M HAZ in part (c).

The BM shows no significant change of the reduction in area with increased hydrogen concentrations (Fig. 9a). This indicates a very good ductility also in case of hydrogen-charged conditions II and III. For example, the reduction in area decreased from 75–78 % in the uncharged condition (I) to 60–65 % at the highest determined hydrogen concentration of approximately 3 ml/100 g Fe (condition III).

Compared to the tempered BM, the non-tempered B HAZ (Fig. 9b) shows a distinct decrease a hydrogen concentration of approximately 1 ml/100 g Fe. At this hydrogen-charged condition, a distinct decrease of the reduction in area is regarded of approximately 30 % when comparing condition I to condition II. This equals to a relative decrease of 80 % compared to the uncharged condition I. In case of severe hydrogen charging (condition III), the reduction in area decreases to 20 %. Hence, it is suggested that 2 ml/100 g Fe can be used as assessment parameter for maximum tolerated hydrogen level in highly stressed B HAZ regions of weld joints due to the strong decrease of the ductility.

The as-quenched M HAZ also shows a distinct loss of reduction in area in hydrogen-charged condition (Fig. 9c). In contrast to the B HAZ, the M HAZ shows a distinct degradation already at hydrogen concentration of 1 ml/100 g Fe (as indicated for condition II). Compared to the uncharged condition I, the reduction in area decreases from 60 to 12 % which corresponds to relative decrease of 80 %. In case of a concentration of 4 ml/100 g Fe (condition III), the reduction in area is below 10 %. This corresponds to a relative loss of 90 %. The distinct degradation of the mechanical properties of the M HAZ is assumed to be related to the achieved high hardness (>400 HV) due to the as-quenched heat treatment condition. This leads to a reduced ductility already in the uncharged condition.

3.1.3 Overview of hydrogen effect on the degradation of the mechanical properties

The following Tables 4 and 5 give a brief overview about the obtained results. Table 4 summarizes the obtained results for the UTS and YS depending on hydrogen concentration and microstructure expressed by the BM grade and the heat-treated HAZ microstructures.

From Table 5, it is seen that only for the M HAZ a distinct degradation of the UTS and YS appears (marked with bold characters). In case of the degradation of the ductility, hydrogen has a remarkable influence as shown in Table 5.

Table 5 summarizes the distinct influence of the hydrogen on the degradation of the mechanical properties in terms of ductility expressed by a decrease of elongation to fracture (A_5) and reduction in area (Z). In other words, the ductility is the most influenced mechanical property in presence of hydrogen. This must be considered in case of evaluation of the susceptibility of those steel grades to a certain hydrogen-related degradation of the mechanical properties. The previous present data support the well-known approach that a hydrogen effect on the degradation

Table 4 Hydrogen effect on the UTS and YS of BM, B HAZ, and M HAZ with corresponding hydrogen concentration

Property	Condition	BM		B HAZ		M HAZ	
		N/mm^2	ml/100 g Fe	N/mm^2	ml/100 g Fe	N/mm^2	ml/100 g Fe
R_m(UTS)	I (H-free)	614	0.0	800	0.0	1349	0.0
	II (H-charged)	638	1.5	790	1.5	1320	1.0
	III (H-charged)	641	3.0	765	3.0	729	2.0
$R_{p0.2}$(YS)	I (H-free)	480	0.0	630	0.0	1001	0.0
	II (H-charged)	530	1.5	650	1.5	1000	1.0
	III (H-charged)	540	3.0	635	3.0	730	3.0

Table 5 Hydrogen effect on the ductility with the corresponding hydrogen concentration

Property	Condition	BM		B HAZ		M HAZ	
		%	ml/100 g Fe	%	ml/100 g Fe	%	ml/100 g Fe
A_5	I (H-free)	22	0.0	18	0.0	15	0.0
	II (H-charged)	20	1.5	10	1.5	6	1.0
	III (H-charged)	12	3.0	2	3.0	2	2.0
Z	I (H-free)	76	0.0	68	0.0	60	0.0
	II (H-charged)	68	1.5	28	1.5	12	1.0
	III (H-charged)	62	3.0	17	3.0	<5	2.0

of the mechanical properties is based on the interaction of hydrogen, microstructure, and load (strain) condition. Hence, the thermal simulation of HAZ microstructures offers the option to rank their susceptibility for hydrogen-assisted degradation of the mechanical properties. By correlating the obtained results for the UTS (R_m), YS ($R_{p0.2}$), the elongation to fracture (A_5), and the reduction in area (Z), it can be ascertained that the as-quenched M HAZ microstructure shows the highest susceptibility for the degradation followed in decreasing order by the non-tempered B HAZ and the tempered BM.

3.2 Fractography

3.2.1 Predominantly fracture topography

The resulting loss of ductility (and in case of M HAZ loss of strength too) for all microstructures can be explained by the different fracture topographies. A general tendency was observed regarding the change in fracture mode from ductile to a mixture of ductile/brittle or mostly brittle depending on the hydrogen concentration and microstructure. From Figs. 10, 11, and 12, the different fracture surfaces are indicated for the BM (Fig. 10), the B HAZ (Fig. 11), and the M HAZ (Fig. 12). In each figure, part (a) indicates the uncharged condition, part (b) indicates moderate charging, and (c) a severe hydrogen-charging condition. All figures show the center region of the fracture surface.

The SEM examinations showed five different fracture topographies depending on the microstructure and the hydrogen concentration. Table 6 shows a brief survey of the occurring fracture topographies and their special characteristics.

Using the abbreviations given in Table 6, the predominantly fracture topography is summarized for all microstructures in Table 7.

As shown in Table 7, the predominantly fracture topography changes with increasing hydrogen concentration compared to the uncharged condition. In general, the fracture topography changes from ductile mode (micro void coalescence) to brittle fracture characterized by QCF around inclusions, CF or IG in case of M HAZ. This indicates that welding

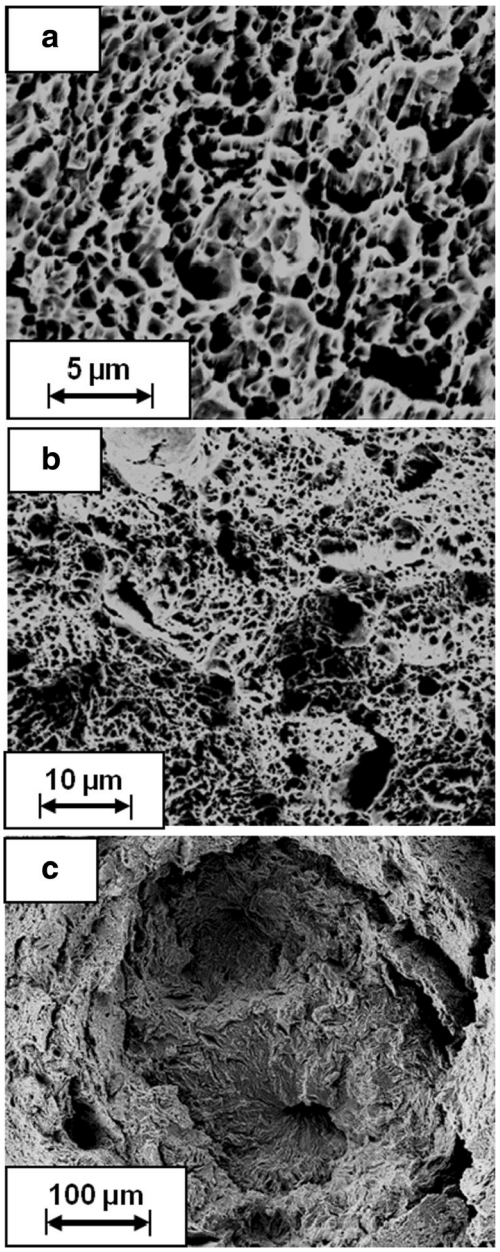

Fig. 10 BM: uncharged (**a**), 1.1 ml/100 g Fe (**b**), and 3.0 ml/100 g Fe (**c**)

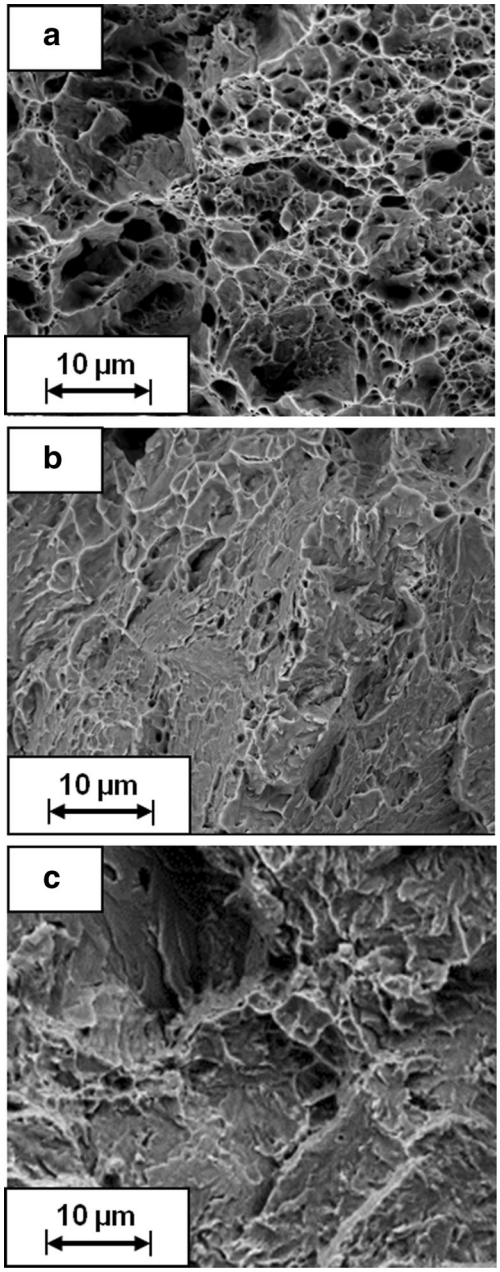

Fig. 11 B HAZ: uncharged (**a**), 1.6 ml/100 g Fe (**b**), and 3.0 ml/100 g Fe (**c**)

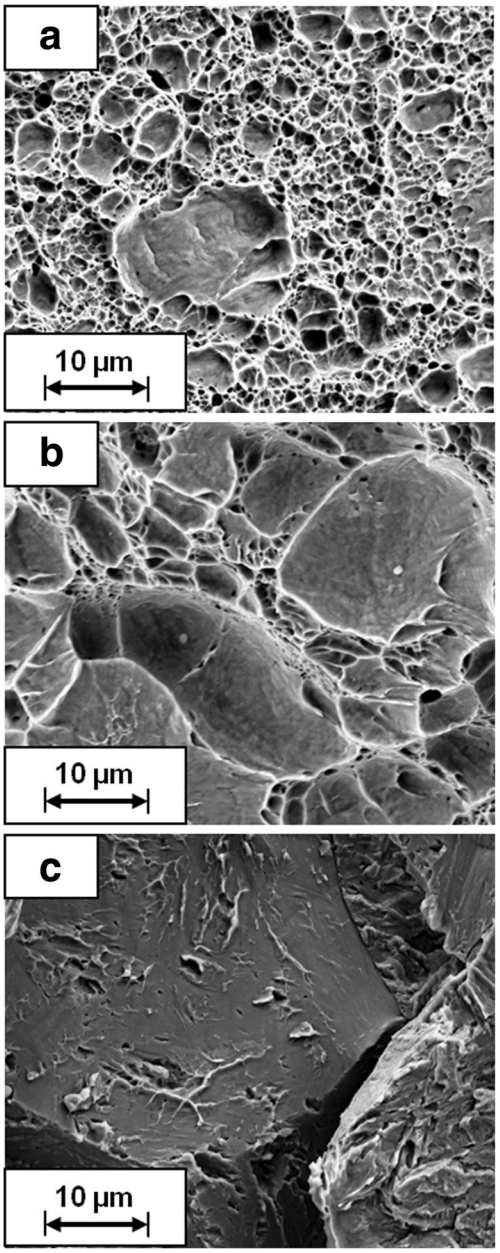

Fig. 12 M HAZ: uncharged (**a**), 0.9 ml/100 g Fe (**b**), and 1.8 ml/100 g Fe (**c**)

thermal cycle (due to the changed cooling time) has great impact on fracture topography occurring in presence of hydrogen. By correlating the determined hydrogen concentrations and the fracture topographies, the ranking of the susceptibility for the degradation is in increasing order BM, B HAZ, and M HAZ. Additionally, this can be correlated to the obtained hardness of 210HV (BM), 276HV (B HAZ), and 448HV (M HAZ). In other words, the occurring hardness can be suggested as an indicator for the susceptibility of a specific microstructure to the degradation of its mechanical properties in case of non heat-treated HAZ.

3.2.2 Quasi-cleavage fracture topography in base material in presence of hydrogen

From Table 7, it can be derived that in uncharged condition for the BM (Fig. 10a), the predominantly fracture topography is ductile characterized by deep dimples (“DD”). It is worth to see that hydrogen concentration of 3.0 ml/100 g Fe changes the fracture topography to a mixture of DD accompanied by QCF (Fig. 10c). This behavior is in agreement with the obtained mechanical properties. The BM grade shows similar fracture topography (or mix) for the surface near region and center region. This indicates a

Table 6 Characteristics of the occurring fracture topographies

Fracture topography	Abbreviation	Characteristics
Ductile	DD or DS	Micro void coalescence or ductile fracture ("DD" for deeper dimples or "DS" for shallower dimples with increased dimple diameter)
Quasi cleavage	QC	Quasi-cleavage facets, characterized by non-smooth fracture surface
Quasi-cleavage facets	QCF	Quasi-cleavage facets around inclusions, surrounded by DD or DS fracture surface, phenomenon is also known as "fish-eye"-forming.
Cleavage fracture	CF	Transgranular cleavage fracture with smooth fracture surface, perpendicular to the load direction.
Intergranular cracking	IG	Fracture along grain boundaries with smooth fracture surface, in some cases accompanied by secondary cracking ("SC")

mostly homogenous hydrogen distribution of hydrogen suggesting sufficient hydrogen-charging time.

In the hydrogen-charged condition, the BM shows a special fracture topography called "fish-eye." The different pictures in Fig. 13 show some typical indications. Thus, Fig. 13a shows the SEM overview figure of the fractured specimen; part (b) shows the magnified central region, and (c) shows the detailed area with the obtained fracture surfaces indicated with QCF and DD/DS.

As shown in Fig. 13c, the typical indications for "fish-eyes" can be identified as an embrittled area with quasi-cleavage fracture (QCF) around inclusions. Additionally, the embrittled area is surrounded by DD fracture. In Fig. 13a–c, the boundary between the DD and the QCF area is indicated with a dashed orange line. It can be determined that several fish-eyes occur (Fig. 13a), and the diameter of the embrittled area is approx. 300 μm (Fig. 13b).

In Fig. 14a, magnified region of a second specimen with an inclusion is shown (indicated with the yellow arrow) which had an average diameter of 10 μm. The corresponding hydrogen concentration in this specimen was determined with 2.4 ml/100 g Fe. The chemical composition of the inclusions was investigated with energy dispersive X-ray spectroscopy (EDX). A typical representative composition is shown in Fig. 14b. The EDX analysis showed that an Al-enriched chemical compound. They are assumed as initiation point for the "embrittled" QCF area.

Table 7 Predominantly fracture topography for the BM, M HAZ, and B HAZ microstructure

Microstructure/position in specimen		Hydrogen level (in ml/100 g Fe)		
		Uncharged	Level I, II: moderate (1–2)	Level III: high (>2)
BM	Center	DD	DD	DD/DS (+QCF)
B HAZ	Center	DD (DS)	DD/DS	QC/CF
M HAZ	Center	DD/DS	DS (+DD)	IG (+SC)

3.2.3 Fracture topography of the HAZ microstructures

In case of the uncharged condition, the fracture mode is ductile for both the HAZ microstructures. The non-tempered bainitic

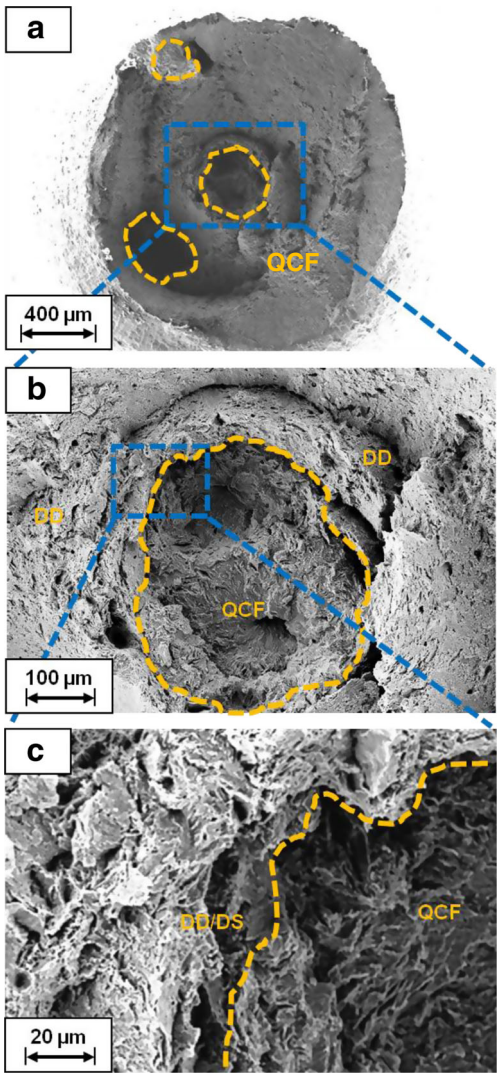

Fig. 13 Fish-eye in BM charged with 3.0 ml/100 g Fe: overview (**a**), magnified central region with QCF facets (**b**), and detail of magnified region (**c**)

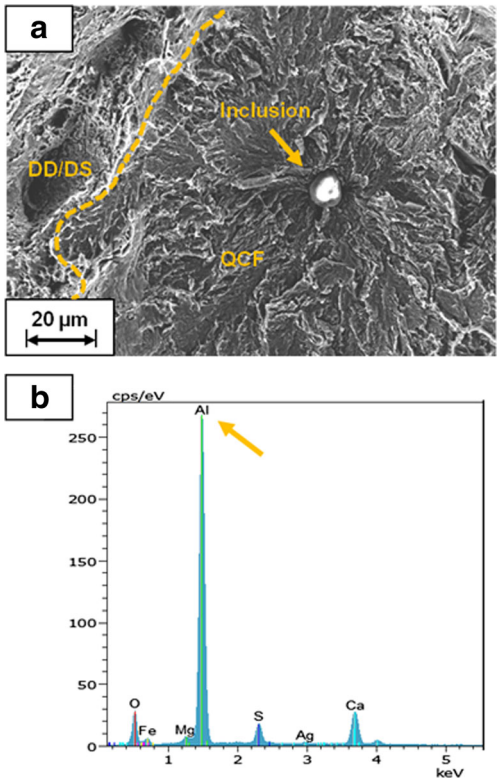

Fig. 14 Fish-eye in BM charged with 1.3 ml/100 g Fe: overview (**a**) and EDX spectra (**b**)

HAZ is shown in Fig. 11a and the as-quenched martensitic HAZ in Fig. 12a. The major part of the fracture surface of the B HAZ is characterized by fracture with "DD" topography accompanied by small areas of shallow dimples "DS." Only the as-quenched M HAZ shows a distinct mixture of deep shallow dimples (DD/DS) indicating a reduced ductility of the material in hydrogen-free condition. Compared to the BM, both the HAZ microstructures showed small areas of shallow dimples indicating a slight reduced ductility. This behavior is in agreement with the obtained mechanical properties (for example the decrease of the reduction in area BM: 76 % vs. both HAZ with 60 to 68 %) and could be related to the higher hardness of the HAZ microstructures accompanied by a missing sufficient heat treatment of the weld joint.

At the moderate hydrogen concentration, the ductile fracture mode shows a mixture of DD and DS for the both HAZ microstructures characterized by micro void coalescence. But compared to the uncharged condition, especially, the as-quenched martensitic HAZ showed distinct appearance of DS in presence of hydrogen (see Fig. 12b—indicated by shallow dimples with larger diameter). This indicates the strong influence of hydrogen on the degradation effect under mechanical load. In addition, the bainitic HAZ (Fig. 11b) showed a "decrease" of the typical deep dimples at hydrogen concentration of 1.6 ml/100 g Fe, too. However, the bainitic HAZ showed minor strong influence on the fracture mode compared to that in the hydrogen-free condition. This indicates that a sufficient heat treatment (tempering) is necessary, in order to decrease the susceptibility for hydrogen-related degradation of the mechanical properties. Hence, a microstructure having a high hardness is assumed to be more susceptible for a degradation of the mechanical properties.

At the high hydrogen concentration, the fracture topography of the non-tempered bainitic HAZ (Fig. 12c) changed to distinct cleavage cracking (accompanied by local areas of shallow dimples—"DS"). Additionally, the as-quenched martensitic HAZ (Fig. 12c) microstructure shows a distinct intergranular cracking ("IG") accompanied by secondary cracking ("SC"). This fracture topography indicates that the (as-quenched) martensitic HAZ shows the highest degradation of the mechanical properties in presence of hydrogen. Hence, it is assumed that this microstructure has the lowest resistance to HAC due to the remarkable degradation of the mechanical properties. Additionally, the obtained fracture surface data support that the hydrogen-charging parameters are sufficient due to observed changes in the fracture topographies compared to those in the uncharged condition.

4 Discussion

4.1 Mechanical properties

The conducted tensile test using hydrogen-free and hydrogen-charged tensile specimens revealed a general tendency for the influence of hydrogen on the mechanical properties in correlation to the (simulated) microstructures. In general, it was ascertained, that hydrogen affects the mechanical properties more in terms of ductility than in tensile strength. Additionally, the initial microstructure (tempered vs. as-quenched) has great impact on the extent of degradation in presence of hydrogen. It has to be mentioned that experimental results could be more or less affected by the applied strain rate. Rehrl et al. [29] reported a remarkable effect of the strain rate on the degradation of mechanical properties in the presence of hydrogen for different high strength steels. They conclude that the hydrogen diffusivity has distinct influence on cracking susceptibility. Hence, in case of a high strain rate ($20*s^{-1}$), the hydrogen diffusion is too low into highly strained regions in the bulk material, i.e., to the crack tip. This means "critical" hydrogen concentrations for remarkable degradation cannot be reached. If the strain rate is very low ($10E\text{-}04*s^{-1}$), the hydrogen has sufficient time for diffusion to the highly strained region. The applied strain rate in our study is approximately $8.3E\text{-}04*s^{-1}$ is in the same range. Hence, possible hydrogen diffusion effects due to the applied strain rate are neglected. Additionally, the strain rate dependency supports the so-called HELP mechanism (hydrogen-enhanced localized plasticity and mechanism) suggested by

Birnbaum and Sofronis [30] assuming that hydrogen accumulates in highly strained regions hindering the dislocation motion and the material partly plasticizes.

4.1.1 Base material

The results presented from our study are in good agreement to reported literature data. Takaku and Kayano [15, 16] investigated the influence of hydrogen on the tensile properties for a RPV steel grade. They showed that a hydrogen concentration of 2 ppm (approx. 2.2 ml/100 g Fe) has no remarkable effect of hydrogen on the tensile strength but the elongation to fracture decreased from 25 to 20 % which fits well to our results. Uhlemann et al. [17] reported a minor importance of hydrogen on the UTS and YS but a major influence in terms of decreased ductility. In their study, the reduction in area decreased from 75 to 55 % in case of a hydrogen concentration of 1.4 ppm (approximately 1.2 ml/100 g Fe) for an SA 508 Cl. 3 but in case of in-situ charging. Wu et al. [11] reported that hydrogen caused a softening of the UTS and a certain loss in ductility. Wu and Kim [18] showed that hydrogen has minor influence on the ultimate tensile strength (R_m). In their study, the presence of hydrogen causes a slight increase of the yield strength ($R_{p0,2}$) and a decrease of elongation to fracture and reduction in area. In our study, we confirmed the general tendency that hydrogen has minor effect on the degradation of the tensile properties compared to the ductility.

4.1.2 Heat affected zone

In our study, we ascertained that the HAZ microstructures show distinct higher tensile properties compared to the tempered BM in the hydrogen-free condition. In case of the non-tempered or as-quenched HAZ, the microstructure shows distinct coarse microstructure with higher hardness compared to the BM indicating a changed precipitate and carbide structure. Hence, different mechanical properties occur compared to the BM. This was also obtained by Kim and Yoon [14]. They examined notched HAZ specimens of multi-pass weld specimens and found higher UTS for the heat-treated (simulated HAZ) microstructures. Additionally, Mark et al. [31] reported higher UTS for the HAZ microstructure of single and three pass weld joints of SA508Cl3 grade. They assume that the increase of the mechanical properties is due to the martensite/bainite mixture in the HAZ microstructure compared to the unaffected BM. This is in accordance with our study.

The achieved mechanical data of the HAZ microstructures in presence of hydrogen are difficult to compare to literature due to lag of available data. But, steel grades with comparable strength and (martensitic) microstructure could be applied for the consideration of the hydrogen effect on the mechanical properties of the HAZ. For example, Oudriss et al. [32] reported a remarkable hydrogen effect on material properties degradation for an AISI 5135 (equals DIN-37Cr4 or AFNOR 38C4). This steel grade has tensile strength of approximately 1350–1400 MPa in the uncharged condition. In presence of dissolute hydrogen, they reported a loss of the ductility of 50 % at a hydrogen concentration of 1.1 to 2.2 ml/100 g Fe. At a hydrogen concentration of 1.5 ml/100 g Fe, an additional decrease of 80 MPa occurred for the tensile strength. These values are in close agreement to the examined as-quenched M HAZ microstructure. Similar results were reported by Yue et al. [33]. A lower hardness decreased the susceptibility for hydrogen-assisted cracking in the HAZ. They concluded that a certain amount of lower bainite improves resistance against HAC compared to a fully martensitic microstructure. Hence, a higher hardness suggests an increased degradation effect on the mechanical properties in presence of hydrogen. This is in accordance with our results. In addition, a part of the authors of the present study examined the hydrogen effect on T24 Cr-Mo-V steel weld microstructures [26]. Although the T24 is a low alloyed Cr-Mo-V steel, it was confirmed that the HAZ is the most susceptible microstructure in terms of hydrogen-affected degradation compared to BM and weld metal. In addition, Blach et al. [20] claim the martensitic HAZ as the most susceptible microstructure for hydrogen-affected degradation. This demonstrates that the HAZ of low alloyed pressure vessel steels, generally independent from the alloy concept, must be considered in case of possible hydrogen uptake. Nevertheless, a possible tempering can improve the mechanical properties of a HAZ. Hence, this effect on the degradation susceptibility in presence of hydrogen should be investigated further.

4.1.3 Evaluation of degradation effect by envelope curves

The UTS R_m and the YS $R_{p0.2}$ are mostly unaffected by hydrogen despite of martensitic HAZ. In contrast, the elongation to fracture and the reduction in area are strongly affected in by hydrogen. To this, calculation of evaluation parameters like the embrittlement index is useful for comparison of different steels and microstructures, as proposed by Depover et al. [12]. This index is defined as so-called embrittlement index EI in accordance to the Eq. 1.

$$\mathrm{EI} = \frac{\mathrm{RA}_u - \mathrm{RA}_c}{\mathrm{RA}_u} \quad (1)$$

Embrittlement index

RA_u is the reduction in area in % for uncharged condition and RA_c in is the reduction in area in % for the hydrogen-charged condition. This procedure allows a qualitative ranking of the different microstructures but unfortunately without mathematical regression method. Hence, another method is applied for the evaluation of the degradation effect of hydrogen on the mechanical properties. Thus, the surface area of the

original crosses section A_0 and the cross section after fracture A_f (adapted reduction in area) is measured by optical microscopy with 5-time magnification. In this special case, it is possible to calculate the so-called true elongation ε_T (Eq. 2).

$$\varepsilon_T = \ln\left(\frac{A_0}{A_f}\right) \quad (2)$$

True elongation [34, 35]

In case of plotting the true elongation versus the hydrogen concentration, a logarithmic value of zero would mean that there is nearly zero ductility left. Then, the hydrogen-related degradation of the material properties (especially the ductility) can be expressed by mathematic approximation of the data plot using exponential functions as envelope curves. This procedure allows mathematical assessing and ranking of the different weld microstructures and their special susceptibility to hydrogen-related degradation. Additionally, the envelope curves represent the hydrogen and the local mechanical load condition as influencing factors. The formulas for the fitted envelope curves for the BM and the both HAZ microstructures are shown in Table 8. Here, LC indicates the lower envelope curve, UC represents the upper envelope curve, and HD means the corresponding measured hydrogen concentration in ml/100 g Fe.

For example, Fig. 15 shows the lower envelope curves for the BM and the obtained B HAZ and MHAZ. The envelope curves are useful for the quantitative transient description of hydrogen effect on the material properties degradation considering the major influence on the ductility. Thus, the hydrogen dependant true elongation describes very well the distinct degradation of the HAZ microstructure compared to the minor influenced BM.

By correlating the envelope curve with numerically calculated values, it is possible to assess certain HAC susceptibility for different weld microstructures [26, 36]. Thus, these regression functions can be implemented in numerical models for HAC based on a certain degradation of the mechanical properties in presence of hydrogen. The principal application of these functions is presented elsewhere [37, 38]. Considering this procedure, the calculation of thermo-mechanical weld stresses and strains can be compared to the envelope curves as cracking criterion for HAC. It is recommended that the LC is used for the numerical calculations due to an assessment as the worst case failure avoiding underestimation of hydrogen

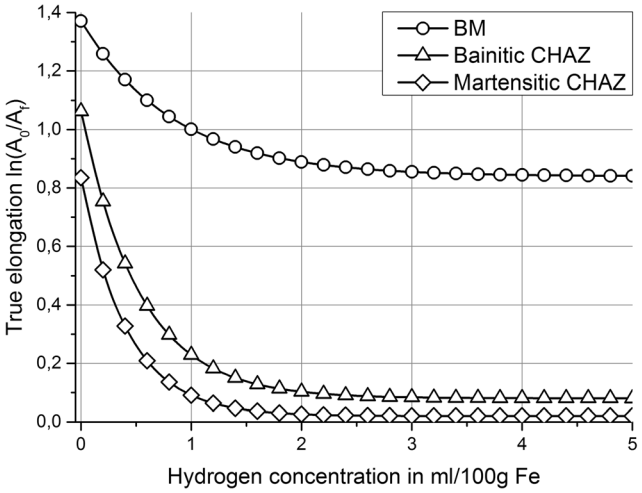

Fig. 15 Lower envelope curves calculated from experimental data

effects on the numerical simulation. Nevertheless, the envelope curves represent a global criterion derived from the tensile tests. They deliver a very good ranking which microstructure should be assessed as most susceptible microstructure for degradation (which can be accompanied by cracking) in presence of quantified hydrogen concentrations. Hence, a local approach for crack initiation needs further investigation.

4.2 SEM investigation

4.2.1 Mechanism of QCF in base material

The embrittled areas (fish-eyes) are characterized by quasi-cleavage fracture (QCF) around Al-rich inclusions and surrounded by ductile fracture surface. According to Lynch [39] and Martin et al. [40], quasi-cleavage fracture is described by non-cleavage planes with fine lines called river markings. The inclusions are assumed as areas of tensile stress concentration fields under mechanical load condition. This means that the lattice is dilated. Hence, these areas are preferred regions for hydrogen diffusion and subsequent accumulation. This is in accordance to the HELP mechanism of Birnbaum and Sofronis [30]. Tsuchida et al. [41] reported that the diameter of embrittled region increases with increasing hydrogen concentration in terms of low-carbon steel. Liu et al. [42] reported for Ni-bearing CrMoV steel embrittled

Table 8 Envelope curves for different microstructures

Microstructure	Lower envelope curve	Upper envelope curve
BM	$\varepsilon_b = 0.531 * e^{-\left(\frac{HD}{0.84}\right)} + 0.84$	$\varepsilon_b = 0.820 * e^{-\left(\frac{HD}{0.21}\right)} + 0.030 * e^{-\left(\frac{HD}{2.20}\right)} + 0.65$
B HAZ	$\varepsilon_b = 0.980 * e^{-\left(\frac{HD}{0.53}\right)} + 0.08$	$\varepsilon_b = 1.130 * e^{-\left(\frac{HD}{1.30}\right)} + 0.10$
M HAZ	$\varepsilon_b = 0.815 * e^{-\left(\frac{HD}{0.41}\right)} + 0.02$	$\varepsilon_b = 0.840 * e^{-\left(\frac{HD}{0.41}\right)} + 0.09$

areas around inclusions. They conclude that the determined inclusions (no chemical composition given) act as initiation points for the embrittled regions. Hence, Al-rich inclusions should be considered as possible crack initiation points in the presence of hydrogen. It has to be mentioned that this special fracture topography was only obtained in the BM. Nevertheless, the tempered condition of the BM in our study indicates that the fish-eye forming has minor effect on determined mechanical properties compared to the as-quenched HAZ microstructures.

4.2.2 Hydrogen dependent fracture topography in the HAZ

The as-quenched bainitic HAZ shows a mixture of cleavage and ductile fracture above a hydrogen concentration of 2.0 ml/100 g Fe. This indicates that the lower hardness of a material is beneficial for decreasing the HAC susceptibility, i.e., the degradation of the mechanical properties. As mentioned, intergranular fracture appeared in presence of hydrogen (1.8 ml/100 g Fe) in the M HAZ. Similar results were obtained by Nagao et al. [43] in lath martensitic steel with an UTS of approximately 1400 MPa. Based on the investigations of Ueji et al. [44], Nagao et al. concluded that hydrogen accumulates at special lattice defects like prior austenite grain boundaries or martensite lath boundaries. The reason is suggested as the hindered dislocation movement and the local dislocation pile up due to increased hydrogen transport by the dislocations. This leads to the formation of intergranular and quasi-cleavage fracture surfaces along the prior austenite grain boundaries. Additionally, they conclude that HAC process depends on the local stress and local hydrogen concentration based on the lattice defects.

In our study, the mentioned fish-eyes in the BM do not appear in the HAZ. It is assumed that a partly dissolution of the Al-rich inclusions occurs due to thermal cycling up to 1200 °C. Nevertheless, the inclusions do not influence the superior mechanical properties of the tempered BM compared to the non-tempered HAZ microstructures. Hence, these inclusions are assumed to play a minor role in the degradation behavior.

5 Conclusions

Hydrogen has a remarkable influence on the mechanical properties which is mainly noticeable by a loss of ductility. In case of welded components, different microstructures like the HAZ appear beside the BM. Especially, in case of welding fabrication of nuclear components, a possible hydrogen degradation effect should be considered for all microstructures. Investigating the mechanical properties, tensile tests were conducted using hydrogen-free and hydrogen-charged specimens. For the evaluation of the weld microstructures, the BM grade and simulated (non-tempered) bainitic and martensitic HAZ were examined. Additionally, selected specimens were analyzed by SEM. The conclusions from the experiments can be summarized as following:

- The non-tempered B and as-quenched HAZ microstructures show an increased UTS and YS in uncharged condition compared to the tempered microstructure of the BM. This is accompanied by decreased ductility (expressed in terms of the reduction in area and elongation to fracture). Additionally, the martensitic HAZ showed a significant increase of the hardness which is responsible for the strong increase of the UTS and YS. In general, the UTS and YS are mostly unaffected in case of the bainitic HAZ and BM condition for the hydrogen-charged specimens. Only in case of martensitic HAZ, a loss of UTS and YS was obtained.
- Hydrogen has a remarkable effect on the ductility (expressed in terms of reduction in area and elongation to fracture) for all the examined microstructures. But, especially, in case of the non-tempered HAZ microstructures, a distinct degradation effect is observed. The degradation in presence of hydrogen is in decreasing order: as-quenched M HAZ, non-tempered B HAZ, and tempered BM. Hence, the (martensitic as-quenched) HAZ is assumed to be the most critical microstructure with higher hardness compared to the BM. Hence, the HAZ is assumed to be the region where hydrogen-assisted cracking preferably occurs. Thus, it is necessary to control the weld heat input carefully to avoid fully martensite microstructure in case of fast cooling (i.e., TIG repair welding in thick-walled components) and the execution of an appropriate heat treatment after welding.
- The SEM investigations showed a ductile fracture mode for all the examined microstructures in the uncharged condition. While in the hydrogen-charged condition, the fracture topography (ductile dimples) changes to (quasi)-cleavage fracture in case of bainitic HAZ and intergranular fracture topography for the martensitic HAZ. This is in accordance with the obtained mechanical data. Additionally, fish-eyes appear in the BM in presence of hydrogen. The Al-rich inclusions are assumed to act as initiation point for the cleavage facets due to stress accumulation around the inclusions under mechanical load. Additionally, in accordance with the literature, the increased stresses are assumed to favor hydrogen transport to highly stressed areas due to the expanded lattice. Nevertheless, this requires further investigations.
- The presented concept of calculating the true elongation is an appropriate concept for the evaluation of the hydrogen-assisted materials degradation. This concept considers the strong influence of the hydrogen on the ductility compared to the tensile strength. Additionally, it can be applied for the quantitative ranking between different (weld) microstructures. Thus, it helps identifying possible critical microstructures which are susceptible for the degradation of mechanical properties and HAC.

Acknowledgments The authors want to thank Mr. Peter Loewe and Steffen Glaubitz for their expertise, and Mr. Romeo Saliwan Neumann for the assistance with the SEM analysis. In particular, the authors want to thank Mrs. Marina Marten and Mr. Michael Richter for their comprehensive assistance for specimen preparation and metallographic analysis. In addition, the authors want to thank Mr. Christophe Primault and Mr. Guillaume Tirand (both Areva NP, France) for the procuration of the examined steels and their assistance in preparing this manuscript.

References

1. Sterne RH, Steele LE (1969) Steels for commercial nuclear power reactor pressure vessels. Nucl Eng Des 10:259–307. doi:10.1016/0029-5493(69)90066-1
2. Davies LM (1999) A comparison of western and eastern nuclear reactor pressure vessel steels. Int J Pres Ves Pip 76(3):163–208. doi:10.1016/S0308-0161(97)00075-6
3. Bocquet P, Cheviet A, Dumont R (1994) Examples of the evolution of the materials for nuclear applications: metallurgical improvement of 16MND5 steel and new technologies for manufacturing heavy components. Nucl Eng Des 151:503–511. doi:10.1016/0029-5493(94)90191-0
4. Chapman T, Offer H, Sanders W, Rusack R (1996) Reduced stress welding process for nuclear plant piping. Nucl Eng Des 170:81–88. doi:10.1016/S0029-5493(97)00014-9
5. Godai T, Okuda N, Yamada M, Yoshino F (1984) Welding consumables for nuclear power plants. Nucl Eng Des 81(2):175–184. doi:10.1016/0029-5493(84)90005-0
6. Kuo HT, Wei RC, Wu WF, Yang YR (2009) Simulated heat affected zone in ASTM A533-B steel plates under low heat inputs. Mater Chem Phys 117:471–477. doi:10.1016/j.matchemphys.2009.06.020
7. Pous-Romero H, Lonardelli I, Cogswell D, Bhadeshia HKDH (2013) Austenite grain growth in a nuclear pressure vessel. Mater Sci Eng A 567:72–79. doi:10.1016/j.msea.2013.01.005
8. Kannengiesser T, Lausch T (2012) Diffusible hydrogen content depending on welding and cooling parameters. Weld World 56(11–12):26–33. doi:10.1007/BF03321392
9. Pitrun M, Nolan D, Dunne D (2004) Diffusible hydrogen content in rutile flux-cored arc welds as a function of the welding parameters. Weld World 48(1–2):2–13. doi:10.1007/BF03266408
10. Schwedler O, Zinke M, Juettner S (2014) Determination of hydrogen contents input in welded joints of press-hardened 22MnB5 steels. Weld World 58:339–346. doi:10.1007/s40194-014-0119-x
11. Wu X, Katada Y, Lee SG, Kim S (2004) Hydrogen involved tensile and cyclic deformation behavior of low-alloy pressure vessel steel. Metall Mater Trans A 35:1477–1486. doi:10.1007/s11661-004-0256-8
12. Depover T, Perez-Escobar D, Wallaert E, Zermout Z, Verbeken K (2014) Effect of hydrogen charging on the mechanical properties of advanced high strength steels. Int J Hydrogen Energ 39(9):4647–4656. doi:10.1016/j.ijhydene.2013.12.190
13. Yu H, Olsen JS, Alvaro A, Olden V, He J, Zhang Z (2016) A uniform hydrogen degradation law for high strength steels. Eng Fract Mech: In press, accepted manuscript. doi:10.1016/j.engfracmech.2016.02.001
14. Kim JH, Yoon EP (1998) Notch position in the HAZ specimen of reactor pressure vessel steel. J Nucl Mater 257:303–308. doi:10.1016/S0921-5093(02)00737-2
15. Takaku H, Kayano H (1982) Combined effects of neutron irradiation and hydrogen absorption on tensile properties and fracture mode of steels for nuclear pressure vessel. J Nucl Mater 110:286–295. doi:10.1016/0022-3115(82)90157-X
16. Takaku H, Kayano H (1978) Hydrogen embrittlement of unirradiated steels for nuclear pressure vessel. J Nucl Mater 78:299–308. doi:10.1016/0022-3115(78)90451-8
17. Uhlemann M, Mueller G, Boehmert J, Ulbricht A (2006) Influence of hydrogen on the toughness of irradiated reactor pressure vessel steels. J Nucl Mater 359:114–121. doi:10.1016/j.jnucmat.2006.08.004
18. Wu XQ, Kim IS (2003) Effect of strain rate and temperature on tensile behavior of hydrogen-charged SA508Cl.3 pressure vessel steel. Mater Sci Eng A 348:309–318. doi:10.1016/S0921-5093(02)00737-2
19. Kim S, Kang SY, Oh SJ, Kwon SJ, Lee S, Kim JH, Hong JH (2000) Correlation of the microstructure and fracture toughness of the heat-affected-zones of an SA508 steel. Metall Mater Trans A 31:1107–1119. doi:10.1007/s11661-000-0106-2
20. Blach J, Falat L, Svec P (2011) The influence of hydrogen charging on the notch tensile properties and fracture behavior of dissimilar weld joints of advanced Cr-Mo-V and Cr-Ni-Mo creep-resistant steels. Eng Fail Anal 18:485–491. doi:10.1016/j.engfailanal.2010.09.043
21. Boellinghaus T, Hoffmeister H, Dangeleit A (1995) A scatterband for hydrogen diffusion coefficients in micro-alloyed low carbon structural steels. Weld World 35(2):83–96
22. Liu Y, Wang M, Liu G (2013) Hydrogen trapping in high-strength martensitic steel after austenized at different temperatures. Int J Hydrogen Energ 38:14364–14368. doi:10.1016/j.ijhydene.2013.08.121
23. Wei FG, Tsuzaki K (2005) Response of hydrogen trapping capability to microstructural change in tempered Fe-0.2C martensite. Scripta Mater 52:467–472. doi:10.1016/j.scriptamat.2004.11.008
24. Zhang L, Kannengiesser T (2014) Austenite grain growth and microstructure control in simulated heat affected zones of microalloyed HSLA steel. Mater Sci Eng A 613:326–335. doi:10.1016/j.msea.2014.06.106
25. Yang JR, Liou SH (1997) Microstructural evolution of simulated heat affected zone in ASTM A533 type B steel plates. Sci Technol Weld Joi 2(3):119–127. doi:10.1179/stw.1997.2.3.119
26. Rhode M, Steger J, Boellinghaus T, Kannengiesser T (2016) Hydrogen degradation effects on mechanical properties in T24 weld microstructures. Weld World 60(2):201–216. doi:10.1007/s40194-015-0285-5
27. Salmi S, Rhode M, Juettner S, Zinke M (2015) Hydrogen determination in 22MnB5 steel grade by use of carrier gas hot extraction technique. Weld World 59:137–144. doi:10.1007/s40194-014-0186-z
28. ISO 3690:2012 Welding and allied processes—determination of hydrogen content in arc weld metal
29. Rehrl J, Mraczek K, Pichler M, Werner E (2014) Mechanical properties and fracture behavior of hydrogen charged AHSS/UHSS grades at high- and low strain rate tests. Mater Sci Eng A 590(10):360–367. doi:10.1016/j.msea.2013.10.044
30. Birnbaum HK, Sofronis P (1994) Hydrogen-enhanced localized plasticity—a mechanism for hydrogen-related fracture. Mater Sci and Eng A 176(1–2):191–202. doi:10.1016/0921-5093(94)90975-X
31. Mark AF, Francis JA, Dai H, Turski M, Hurrell PR, Bate SK, Kornmeier JR, Withers PJ (2012) On the evolution of local material properties and residual stress in a three-pass SA508 steel weld. Acta Mater 60:3268–3278. doi:10.1016/j.actamat.2012.03.022
32. Oudriss A, Fleurentin A, Courlit C, Conforto E, Berziou C, Rebere C, Cohendoz S, Sobrino JM, Feaugas X (2014) Consequence of diffusive hydrogen contents on tensile properties of martensitic steel during desorption at room temperature. Mater Sci Eng A 593:420–428. doi:10.1016/j.msea.2014.01.039
33. Yue X, Feng XL, Lippold JC (2014) Effect of diffusible hydrogen level on heat-affected zone hydrogen-induced cracking of high-strength steels. Weld World 58:101–109. doi:10.1007/s40194-013-0087-6

34. Davies JR (2004) Tensile testing, 2nd edn. ASM-International, Materials Park (OH), USA
35. Dieter GE (1986) Mechanical metallurgy, 3rd edn. McGraw-Hill, New York
36. Zimmer P, Kannengiesser T, Boellinghaus T (2004) Effects of hydrogen on weld microstructure mechanical properties of the high strength steels S690Q and S1100QL. IIW-Doc II-1525-04
37. Wongpanya P, Boellinghaus T, Lothongkum G, Hoffmeister H (2009) Numerical modeling of cold cracking initiation and propagation in S 1100 QL steel root welds. Weld World 53(3–4):R34–R43. doi:10.1007/BF03266701
38. Mente T, Boellinghaus T, Schmitz-Niederau M (2012) Heat treatment effects on the reduction of hydrogen in multi-layer high-strength weld joints. Weld World 56(7–8):26–36. doi:10.1007/BF03321362
39. Lynch SP (1984) A fractographic study of gaseous hydrogen embrittlement and liquid-metal embrittlement in a tempered-martensitic steel. Acta Metall Mater 32(1):79–90. doi:10.1016/0001-6160(84)90204-9
40. Martin ML, Fenske JA, Liu GS, Sofronis P, Robertson IM (2011) On the formation and nature of quasi-cleavage fracture surfaces in hydrogen embrittled steels. Acta Mater 59(4):1601–1606. doi:10.1016/j.actamat.2010.11.024
41. Tsuchida Y, Watanabe T, Kato T, Seto T (2010) Effect of hydrogen absorption on strain-induced low-cycle fatigue of low carbon steel. Proc Eng 2(1):555–561. doi:10.1016/j.proeng.2010.03.060
42. Liua Q, Irwantob B, Atrensa A (2013) The influence of hydrogen on 3.5NiCrMoV steel studied using the linearly increasing stress test. Corros Sci 67:193–203. doi:10.1016/j.corsci.2012.10.019
43. Nagao A, Smith CD, Dadfarnia D, Sofronis P, Robertson IM (2014) Interpretation of hydrogen induced fracture surface morphologies for lath martensitic steel. Proc Mater Sci 3:1700–1705. doi:10.1016/j.mspro.2014.06.274
44. Ueji R, Tsuji N, Minamino Y, Koizumi Y (2002) Ultragrain refinement of plain low carbon steel by cold rolling and annealing of martensite. Acta Mater 50(16):4177–4189. doi:10.1016/S1359-6454(02)00260-4